THE JOURNAL OF PHYSICAL CHEMISTRY C
A JOURNAL OF THE AMERICAN CHEMICAL SOCIETY

pubs.acs.org/JPCC

Article

Resolving Complex Photoconductivity of Perovskite and Organic Semiconductor Films Using Phase-Sensitive Microwave Interferometry

Jasleen K. Bindra, Pragya R. Shrestha, Sebastian Engmann, Chad Cruz, Lea Nienhaus, Emily G. Bittle, and Jason P. Campbell*

Cite This: *J. Phys. Chem. C* 2023, 127, 4203−4209

Read Online

ACCESS | Metrics & More | Article Recommendations | Supporting Information

ABSTRACT: Complex transient photoconductivity ($\Delta\sigma$) contains rich fingerprints of charge recombination dynamics in photoactive films. However, a direct measure of both real ($\Delta\sigma'$) and imaginary ($\Delta\sigma''$) components has proven difficult using conventional cavity-based time-resolved microwave conductivity approaches. Here, we present a novel approach to resolve $\Delta\sigma'$ and $\Delta\sigma''$ parts of $\Delta\sigma$ by using a nonresonant coplanar transmission line and a microwave interferometric detection scheme. The use of a phase-sensitive microwave interferometer greatly increases the measurement sensitivity and eliminates the requirement of a resonant cavity. This broadband detection scheme allows for direct measurement of $\Delta\sigma$. The relationship between the experimental phase shift and $\Delta\sigma'$ and $\Delta\sigma''$ components is decoded through an in situ electron spin resonance (ESR) measurement. ESR line shape analysis is used to confirm the assignment of the transients to the $\Delta\sigma'$ and $\Delta\sigma''$ components. We demonstrate the utility of this technique on thin films of poly(3-hexylthiophene): [6,6]-phenylC61-butyric acid methyl ester (P3HT:PCBM) and perovskite $MA_{0.85}FA_{0.15}PbI_3$ films on glass.

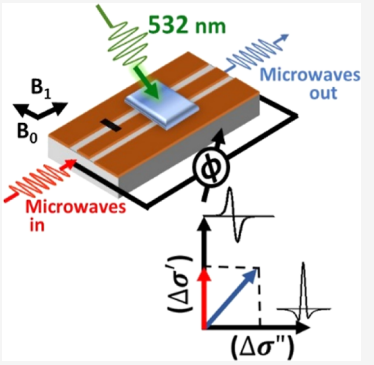

INTRODUCTION

Time-resolved microwave conductivity (TRMC) is an experimental technique used to record the transient light-induced changes in the conductance of photoactive thin films with nanosecond time resolution.[1−4] The change in conductance due to the photo-generated charge carrier dynamics introduces a time-dependent impedance change that can be probed using typical microwave impedance detection schemes.[1−4] This knowledge of charge-carrier dynamics in semiconductors is important for understanding the electronic and material properties of a system. It is also valuable in device design and optimization. This is particularly crucial for organic semiconductor-based solar cells, light-emitting diodes, and transistors, where charge generation, extraction, and amplification, respectively, are highly dependent upon the dynamics of the photogenerated carriers.[5−7] In contrast to the alternative techniques like time of flight measurements,[8−11] field effect transistors measurements,[12] or photo-induced charge extraction by a linearly increasing voltage,[13−17] TRMC is a contactless technique that avoids the necessity to apply ohmic contacts and therefore eliminates effects due to active layer−contact interfaces.[1−4]

A conventional cavity-based TRMC setup relates the total impedance change to a measure of the total complex photoconductivity ($\Delta\sigma$) and cannot directly distinguish between the real ($\Delta\sigma'$) and imaginary ($\Delta\sigma''$) components.[1−4] Some attempts have been made by several groups to resolve $\Delta\sigma$ with varying degrees of success.[18−21] The work presented here circumvents many of the experimental hurdles in observing the complex transient impedance changes using cavity-based detection schemes by utilizing a microwave interferometric detection scheme.[22] To sense small impedance changes, the microwave interferometric detection circuit is coupled to semiconducting thin films through a coplanar transmission line probe. A nanosecond pulsed laser is used to photogenerate charge carriers in these films. A microwave phase shifter in the homodyne demodulation scheme is used to directly select $\Delta\sigma'$ and $\Delta\sigma''$ components of $\Delta\sigma$. Line shape analysis of a simultaneous electron spin resonance (ESR) measurement provides a methodology to decode the relationship between the experimentally variable microwave phase and the $\Delta\sigma'$ and $\Delta\sigma''$ components. The use of the phase-sensitive microwave interferometric detection scheme has the following advantages over the conventional (cavity-based) TRMC setup approaches: (1) There is a capability to experimentally resolve $\Delta\sigma$ without complicated frequency dispersion analysis.[18] (2) The measurement sensitivity is independent of the cavity loading and is instead determined by the interferometric

Received: December 12, 2022
Revised: February 3, 2023
Published: February 17, 2023

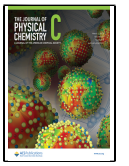

https://doi.org/10.1021/acs.jpcc.2c08700
J. Phys. Chem. C 2023, 127, 4203−4209

tuning. (3) Use of a sensitive microwave interferometer with a typical averaging (10 to 1000) allows measurement of the TRMC signal with a signal-to-noise ratio > 150.[22] The time resolution of this measurement (~0.1 ns) is limited by the rise time (~2 ns) of the laser pulse which are both far faster than the time scale of the transient photoconductivity in most organic semiconductors. This enables us to investigate device-sized (~nL) volumes of semiconducting films. The decrease in the probed area allows for more direct comparisons with working devices as contrasted with the stacked films used to obtain sufficient signal in the standard microwave cavity technique, where film-to-film variation may influence results. (4) There is the ability to conduct simultaneous impedance and ESR measurements, which would not be possible in a resonant cavity that can only concentrate either electric or magnetic fields. (5) Concurrent measurement of a known ESR line shape, for example, using 2,2-diphenyl-1-picrylhydrazyl (DPPH), can confirm the assignment of the obtained transients to the pure $\Delta\sigma'$ and $\Delta\sigma''$ components.

EXPERIMENTAL SECTION

P3HT:PCBM. P3HT:PCBM thin films of poly(3-hexylthiophene) (P3HT, >98% head-to-tail regioregularity) and [6,6]-phenylC61-butyric acid methyl ester (PCBM) were used. Solutions of 20 mg/mL total solid content, with 1:1 weight ratio P3HT:PCBM, were prepared in chlorobenzene. Films were prepared by spin-coating at 17 rev/s onto glass substrates, followed by an annealing step, 300 s at 150 °C, inside a nitrogen-filled glovebox (<0.1 ppm O_2, <0.1 ppm H_2O).

$MA_{0.85}FA_{0.15}PbI_3$. $MA_{0.85}FA_{0.15}PbI_3$ (MAFA) thin films were fabricated as described elsewhere.[23] Briefly, glass substrates were cleaned by sonication in 2% alkaline concentrate, water, and ethanol separately, followed by UV–ozone treatment. Precursor solutions were prepared in anhydrous dimethyl formamide/dimethyl sulfoxide (9:1, v/v): PbI_2 (1.2 mol/L), methyl ammonium iodide (1.2 mol/L), and formamidinium iodide (1.2 mol/L). Following dilution to 0.6 mol/L, ~100 nm metal-halide perovskite (MHP) thin films were created in a two-step spin-coating process: 17 rev/s for 10 s and 85 rev/s for 30 s with anhydrous chlorobenzene as the antisolvent. The resulting films were annealed at 110 °C for 900 s.

DPPH Infused Paper. 2,2-diphenyl-1-picrylhydrazyl (DPPH) sample is prepared by dipping a piece of copy paper in a high concentration 10 wt % acetone/DPPH solution. Upon drying, DPPH-infused paper of size ~1 mm × 1 mm was secured on the transmission line with adhesive tape.

RESULTS AND DISCUSSION

Microwave Conductivity Setup. A schematic of the TRMC system used in this study is shown in Figure 1. Thin films of photosensitive materials on glass substrates are affixed to a coplanar transmission (no ground plane) line which efficiently couples microwave electric and magnetic fields into the samples (Figure 2A). The transmission line has a characteristic impedance of 50 Ω. Figure 2B shows the cross-section of the transmission line with the spatial distribution of the electric fields. The TRMC measurements rely on electric field coupling to the photoactive sample to sense the change in photoconductivity, while the ESR measurements rely on the magnetic field coupling to sense the spin transitions in DPPH. Detection occurs in transmission mode (rather than the reflection mode) with the transmission line structure inserted into the "sample arm" of the microwave interferometer[22] circuit which operates at X-band frequencies (8–12 GHz).

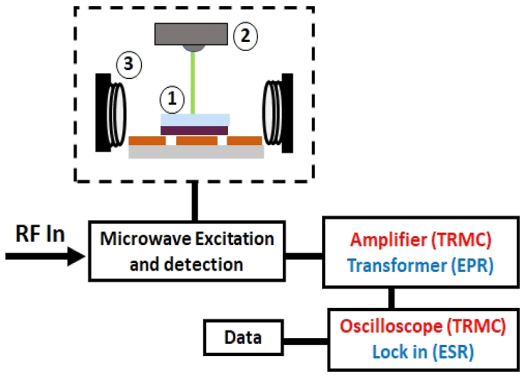

Figure 1. Experimental TRMC and ESR setup with phase-sensitive detection scheme showing microwave excitation and detection circuitry. Inset shows the sample assembly with transmission line and sample film (1), light source (2), and electromagnet with coils (3).

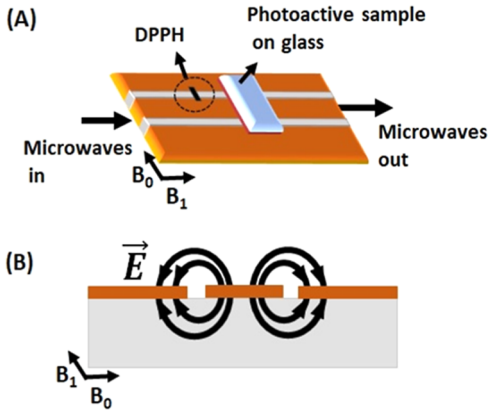

Figure 2. (A) Transmission line connected to the microwave excitation and detection circuit with photo-active material film on glass and an ESR probe (DPPH-infused paper) secured on it. (B) Cross-section of the transmission line with spatial distribution of the electric field. Time-varying magnetic field is perpendicular to the electric field.

Scheme 1. Phase Detection Using an X-Band Mixer

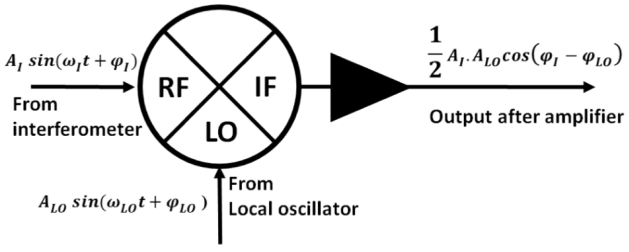

The microwave interferometer is assembled in a Mach-Zehnder configuration[22] which is tuned to null the output in the absence of a transient photoconductivity impedance change. The output of the microwave interferometer is amplified and then demodulated (homodyne) to reveal the transient impedance change. A trombone line microwave phase shifter is inserted in the local oscillator (LO) arm of the demodulation scheme. This phase shifter provides the experimental phase control required to select the in-phase

https://doi.org/10.1021/acs.jpcc.2c08700
J. Phys. Chem. C 2023, 127, 4203–4209

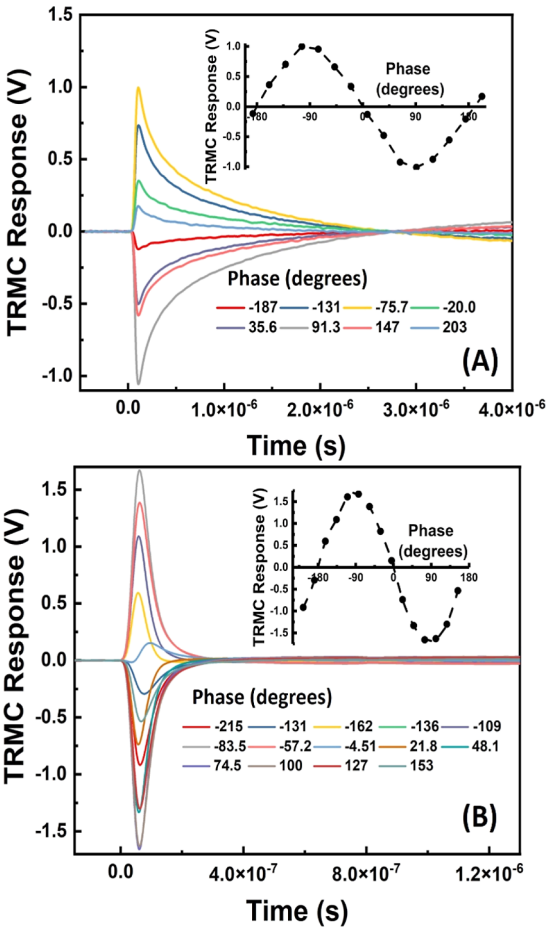

Figure 3. TRMC transients obtained at different microwave phases for (A) drop-casted P3HT:PCBM (50:50) and (B) 100 nm spin-coated MAFA films on glass. Insets: microwave phase dependence of transient amplitudes (measurement error bars are smaller than the data points).

and out-of-phase components of $\Delta\sigma$. The demodulated transient signals are then amplified and recorded by a high-resolution oscilloscope. Samples were illuminated using the second harmonic (532 nm) of a pulsed Nd:YAG laser with an excitation intensity of 10 μJ/cm^2/pulse, a pulse width of 5 ns (FWHM), and a 10 Hz repetition rate. Data acquisition was synchronized using an external photodiode trigger. Though the samples are prepared and stored in an Ar or N_2 environment, all TRMC measurements were performed in ambient air.

Phase-Sensitive Microwave Detector. All components of the interferometric microwave detector employed in this study are described elsewhere.[22] A detailed discussion of the phase-sensitive detection component is presented in this section to elucidate its working principle and how it can be used to resolve the complex conductivity.

The heart of phase-sensitive detection is an X-band mixer (Scheme 1). The output of the mixer is the product of two input signals (RF × LO). The signal exiting the interferometer enters the mixer at the RF port. It is described by

$$S_I = A_I \sin(\omega_I t + \varphi_I) \quad (1)$$

Here, A_I is the amplitude of the interferometer output, φ_I is the frequency of the input microwaves, and the phase delay ω_I is a result of microwave absorption through the semiconducting film. The absorption is related to the complex conductance of the film.

The phase shifter on the LO path allows one to change the phase of the LO microwave signal. Therefore, the signal to the LO input of the mixer can be described by

$$S_{LO} = A_{LO} \sin(\omega_{LO} t + \varphi_{LO}) \quad (2)$$

Here, A_{LO} is the amplitude of the LO microwave signal, $\omega_{LO} = \omega_I$, and φ_{LO} is the LO phase. The product output signal of the X-band mixer then contains components at the sum and difference frequencies. This can be described as

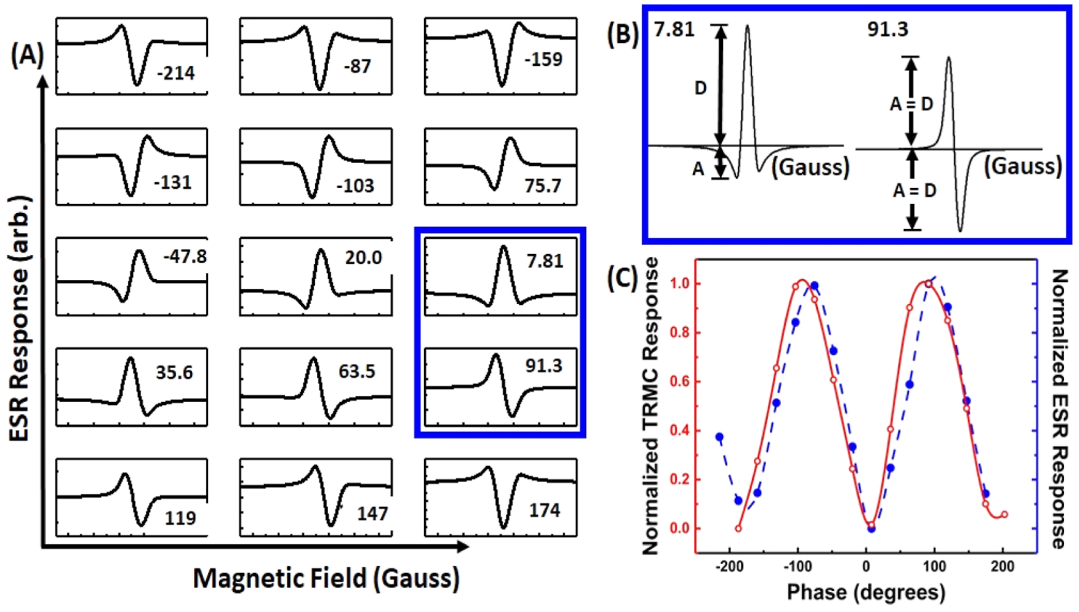

Figure 4. (A) ESR microwave phase dependence for DPPH. (B) Blue box indicates line shapes which are nearly 90° out of phase and approximate absorption and dispersion ESR signals. (C) Normalized absolute TRMC (red) amplitude and normalized A % obtained from ESR measurement at different microwave phases (blue) (measurement error bars are smaller than the data points).

https://doi.org/10.1021/acs.jpcc.2c08700
J. Phys. Chem. C 2023, 127, 4203−4209

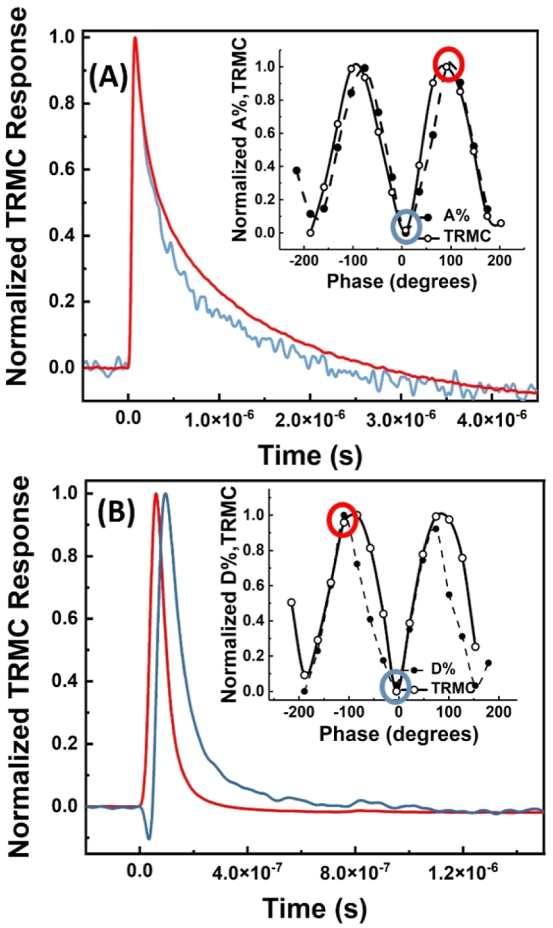

Figure 5. TRMC transients obtained at nπ (blue) and π(n+1/2) (red) microwave phases. (A) Drop-casted P3HT: PCBM (50: 50) and (B) 100 nm spin-coated MAFA films on glass. Insets: Normalized absolute TRMC amplitude and normalized A % or D % obtained from ESR measurement at different microwave phases (measurement error bars are smaller than the data points).

$$\text{output} = \left(\frac{1}{2}\right)A_I A_{LO}\{\cos(\varphi_I - \varphi_{LO}) - \cos(2\omega_I t + (\varphi_I + \varphi_{LO}))\} \quad (3)$$

In the homodyne arrangement, the component arising from the frequency difference is quasi-DC and depends only upon the input amplitudes and phase differences, while the component arising from the sum frequencies is twice the input frequency. Since the higher frequency component ($2\omega_I$) is outside the bandwidth of the amplifier, (3) reduces to

$$\text{output}\ (\omega_I = \omega_{LO}) = \left(\frac{1}{2}\right)A_I \cdot A_{LO}\ \cos(\varphi_I - \varphi_{LO}) \quad (4)$$

where

$$\text{output} = \begin{cases} \left(\frac{1}{2}\right)A_I A_{LO}\ \cos(\varphi_I) & \text{for } \varphi_{LO} = 0 \\ -\left(\frac{1}{2}\right)A_I A_{LO}\ \sin(\varphi_I) & \text{for } \varphi_{LO} = (\pi/2) \end{cases} \quad (5)$$

The outputs given in eq 5 for $\varphi_{LO} = 0$ and $\varphi_{LO} = \pi/2$ are the in-phase and out-of-phase components of eq 1 with respect to the LO frequency. These components are related to the real and imaginary parts of the complex conductance. Thus, the LO phase can be used as an experimental variable to separate the real and imaginary components of a complex signal using this phase-sensitive detection. However, the phase, φ_I, of the microwave entering the RF port of the mixer (coming from the interferometer) is dependent on sample placement, interferometer tuning, and microwave amplification. Thus, there is a requirement to decode the phase relationship between the microwave signals entering the RF and LO ports of the mixer.

ESR Setup. To decode the phase relationship between microwave signals to the mixer and the TRMC transient, the TRMC setup can be readily converted to an operando continuous wave ESR measurement setup to perform in situ ESR measurements. This only requires the addition of an electromagnet capable of supporting X-band ESR measurements (~300 mT), magnetic field modulation coils sufficient to support conventional lock-in detection schemes (~0.3 mT @ 30 kHz) (Figure 1), and a standard ESR reference sample consisting of DPPH-infused paper secured on the transmission line adjacent to the photoactive TRMC sample. The whole transmission line sample holder assembly is centered within the poles of the electromagnet (Figure 1). In the ESR measurement, the output of the microwave interferometer is demodulated and processed through second-phase sensitive detection (lock-in amplifier) to yield the magnetic field-modulated ESR response. Analysis of the ESR line shape of the DPPH standard spectrum provides a direct measure of the phase relationship between microwaves exiting the interferometer (RF port of the mixer) and those on the LO port. This allows one to select the absorptive or dispersive line shape (delineating in and out of phase detection, respectively) of the ESR response and correlate that with the $\Delta\sigma'$ and $\Delta\sigma''$ components of TRMC response.

The further advancement of high-efficiency organic photovoltaics (OPVs) requires understanding of the complex processes involved in the photogeneration of charges[24,25] in device analogous samples. One of the most studied binary polymer, fullerene systems, for OPVs consists of a blend of regioregular P3HT and the electron acceptor PCBM. While the rate of exciton dissociation in P3HT:PCBM blends is known to occur on an ultrafast time scale (~tens to hundreds of femtoseconds), the significantly longer (hundreds of nanoseconds or longer) charge recombination process ultimately determines the device performance.[1] Therefore, TRMC is an ideal tool to investigate carrier dynamics in the nanosecond to sub-microsecond time regime. Further, the use of a suitable model allows one to distinguish between carrier trapping, primary geminate recombination, and second-order carrier recombination.[1,20]

Another material of interest for photovoltaic applications is the MHP, MAFA. This ionic semiconductor is known to exhibit a large relative permittivity ($\varepsilon_r \sim 5-50$).[26] Giant dielectric constant modulation has been reported in MHPs, where ε_r increases by 3 orders of magnitude under illumination from 1 sun conditions at kHz to MHz frequencies.[27] Therefore, this material is expected to show distinct in-phase and out-of-phase TRMC transients at these frequencies.[28] In this system, the optical dielectric response due to dielectric permittivity is known to occur over tens to hundreds of picoseconds.[26] TRMC, with nanosecond time resolution, is an ideal tool to probe the slower orientational components[26] due to the realignment of dipolar species and the space charge contribution that results from free charges (both ionic and

https://doi.org/10.1021/acs.jpcc.2c08700
J. Phys. Chem. C 2023, 127, 4203−4209

electronic) redistributing over macroscopic distances in the material. In this work, we use the TRMC to evaluate photo-induced changes in the relative permittivity [$\Delta\varepsilon_r(t) \propto \Delta\sigma(t)$] as a function of time for a 100 nm thin film of MAFA.

During a TRMC experiment, the sample is optically excited by a 532 nm laser with an excitation intensity of 10 μJ/cm^2/pulse and a pulse width of 5 ns. Microwave propagation through the sample is monitored by the interferometer detection circuit, and the transient decay of the output signal is recorded as a function of time. The duration and nature of the subsequent decay enable one to probe the dynamics of carrier recombination. We report the signal difference [$\Delta V(t)$] between measurements taken in the presence and absence of the laser pulse and define this as the TRMC response.

$$\Delta V(t) \propto \Delta\sigma(t) = \Delta\sigma' + i\Delta\sigma'' \quad (6)$$

The gigahertz complex photoconductivity ($\Delta\sigma$) contains the $\Delta\sigma'$ and $\Delta\sigma''$ conductivity parts of the complex photoconductivity. $\Delta\sigma'$ corresponds to the change in the dielectric loss ε'', while $\Delta\sigma''$ represents the change in the real part (ε') of the dielectric constant ε.[29]

The kinetic traces of the drop-casted P3HT:PCBM blend film and 100 nm spin-coated MAFA film for different microwave phases at 8.974 GHz (16 dBm input to the transmission line for P3HT: PCBM and 4 dBm for MAFA films) are shown in Figure 3A,B. The phase dependence of the amplitudes (peak value of the transient) of the recorded transients is shown in Figure 3 insets. The observed change in the transient amplitude with microwave phase clearly indicates the phase dependence of the recorded signal. The observed change in polarity of the transients has been assigned to the signal from the trapped electrons in P3HT:PCBM films.[20] The phase dependence of transient amplitude is recorded at different microwave frequencies (8.5, 8.974, 9.5, 10, and 10.5 GHz). Normalized amplitude versus microwave phase plots for different frequencies are shown in Figure S1. Since the same trombone line phase shifter was used for all frequencies, the phase axis was adjusted for each frequency to make it convenient for direct comparison. Irrespective of the frequency of microwaves, the transient trace with pure $\Delta\sigma'$ was recorded at π(n+1/2), and pure $\Delta\sigma''$ component was recorded at nπ microwave phase (Figure S1). An in situ ESR measurement is used to confirm this assignment.

During an ESR measurement at resonance, the magnetic susceptibility, $\chi = \chi' + j\chi''$, changes both χ' and χ'' parts in conformity with Kramers−Kronig relations.[30] Therefore, any change in the microwave phase should be reflected in the line shape of the recorded ESR signal. A pure dispersion (χ') or pure absorption signal (χ'') can be obtained by tuning the microwave phase. The ESR absorption line shape is recorded as the first derivative of the Lorentzian for purely absorption, and the second derivative indicates the dispersion signal.

A simple ESR dispersion and absorption line shape analysis (DISPA)[30,31] is used to determine the phase relationship between the RF and LO signals and experimentally validate the relation between $\Delta\sigma'$ and $\Delta\sigma''$ components of complex photoconductivity. Figure 4A illustrates the ESR line shapes for the DPPH-infused paper as a function of the microwave phase difference between the RF and LO signals (ESR microwave phase dependence for the MAFA thin film is shown in Figure S2). The change of line shapes from absorption [Figure 4B (left)] to dispersion [Figure 4B (right)] and all intermediate mixed line shapes are observed. In the empirical DISPA analysis, the first derivative ESR signal is separated to components above and below the baseline and can be characterized by "A" and "D" amplitude parameters (defined in Figure 4B). In this framework, pure absorption occurs when the total amplitude is equally split between "A" and "D" components (A = D). Dispersion line shapes have the minimum "A" component of the total amplitude. Similarly, mixed line shapes can be deduced by monitoring the percentage of "A" component in the total line shape amplitude. The phase dependence of the normalized A % obtained from DISPA analysis follows the microwave phase dependence of the normalized absolute TRMC amplitude as shown in Figure 4C. This allows us to assign TRMC transients to the $\Delta\sigma'$ and $\Delta\sigma''$ components of complex photoconductivity based on the recorded ESR line shape.

Figure 5 shows the kinetic traces corresponding to $\Delta\sigma'$ and $\Delta\sigma''$ of P3HT:PCBM (Figure 5A) and 100 nm MAFA films (Figure 5B). The phase dependence of absolute transient amplitudes obtained from TRMC measurements and corresponding DISPA analysis from operando ESR measurements are shown in the respective insets. It should be noted that the microwave phase dependence of the normalized absolute TRMC amplitude follows phase dependence of the normalized A % obtained from DISPA analysis for P3HT:PCBM films, but for MAFA, it follows D %. The P3HT:PCBM films display identical transients for $\Delta\sigma'$ and $\Delta\sigma''$ obtained at nπ and $\pi(n + 1/2)$ microwave phases. However, the transients obtained for nπ and $\pi(n + 1/2)$ microwave phases for the MAFA film (Figure 5B) are comparatively mismatched. The mismatch of the transients obtained for nπ and $\pi(n + 1/2)$ microwave phases for the MAFA film over the microsecond time range suggests kinetic differences in $\Delta\sigma'$ and $\Delta\sigma''$. Similar differences between the real and imaginary photoconductive decays were also observed in previous studies of polycrystalline MAFA films.[27] The frequency regime we probe in these experiments (~10 GHz) is associated with molecular motions of A-site cations.[28] This motion of the A-site cations and polaronic charges contribute to the imaginary component of conductivity and the relative magnitude of $\Delta\sigma'$ and $\Delta\sigma''$ in perovskites.

CONCLUSIONS

In conclusion, using the microwave interferometer-based phase-sensitive detection scheme with a coplanar transmission line, we have carried out TRMC and ESR measurements for photo-active thin films at different microwave phases for small volume samples. By studying the P3HT:PCBM and MAFA thin films as examples, we have demonstrated that this TRMC approach can be used not only to extract complex conductivity but also to experimentally resolve the complex photoconductivity. Use of operando ESR further allows one to confirm the assignment of TRMC transients to the real or imaginary components. P3HT:PCBM films show changes in conductivity consistent with previous results of photocurrent generation. In MAFA, we can observe changes in complex conductivity related to photo-induced ionic motion related to previously observed A-site cation motions. Hence, this approach has the potential to extend the utility of TRMC measurements in organic/ionic semiconducting materials.

ASSOCIATED CONTENT

Supporting Information

The Supporting Information is available free of charge at https://pubs.acs.org/doi/10.1021/acs.jpcc.2c08700.

https://doi.org/10.1021/acs.jpcc.2c08700
J. Phys. Chem. C 2023, 127, 4203−4209

TMRC amplitude phase dependence for different microwave frequencies and ESR microwave phase dependence for the MAFA thin film (PDF)

AUTHOR INFORMATION

Corresponding Author

Jason P. Campbell − *Nanoscale Device Characterization Division, National Institute of Standards and Technology, Gaithersburg, Maryland 20899-3460, United States;* orcid.org/0000-0002-3406-1165; Email: jason.campbell@nist.gov

Authors

Jasleen K. Bindra − *Nanoscale Device Characterization Division, National Institute of Standards and Technology, Gaithersburg, Maryland 20899-3460, United States; Institute for Research in Electronics and Applied Physics, University of Maryland, College Park, Maryland 20742, United States;* orcid.org/0000-0001-7031-7482

Pragya R. Shrestha − *Nanoscale Device Characterization Division, National Institute of Standards and Technology, Gaithersburg, Maryland 20899-3460, United States; Theiss Research, La Jolla, California 92037, United States;* orcid.org/0000-0001-9499-7822

Sebastian Engmann − *Nanoscale Device Characterization Division, National Institute of Standards and Technology, Gaithersburg, Maryland 20899-3460, United States; Theiss Research, La Jolla, California 92037, United States*

Chad Cruz − *Nanoscale Device Characterization Division, National Institute of Standards and Technology, Gaithersburg, Maryland 20899-3460, United States*

Lea Nienhaus − *Department of Chemistry, Florida State University, Tallahassee, Florida 32306, United States;* orcid.org/0000-0003-1412-412X

Emily G. Bittle − *Nanoscale Device Characterization Division, National Institute of Standards and Technology, Gaithersburg, Maryland 20899-3460, United States;* orcid.org/0000-0002-6254-1692

Complete contact information is available at: https://pubs.acs.org/10.1021/acs.jpcc.2c08700

Author Contributions

The manuscript was written through contributions of all authors.

Funding

Any funds used to support the research of the manuscript should be placed here (per journal style).

Notes

The authors declare no competing financial interest.

ACKNOWLEDGMENTS

L.N. acknowledges funding from the Florida State University. J.K.B. acknowledges support under the Cooperative Research Agreement between the University of Maryland and the National Institute of Standards and Technology Physical Measurement Laboratory, award 70NANB18H165, through the University of Maryland. Valuable guidance and discussions were provided by Dr. D. J. Gundlach, Dr. N. Abhyankar, and Dr. K.P. Cheung at the National Institute of Standards and Technology.

ABBREVIATIONS

TRMC	time resolved microwave conductivity
ESR	electron spin resonance
P3HT	PCBM, poly (3-hexylthiophene: [6,6]-phenylC61-butyric acid methyl ester
MAFA	$MA_{0.85}FA_{0.15}PbI_3$
DPPH	2,2-diphenyl-1-picrylhydrazyl
DISPA	dispersion and absorption line shape analysis

REFERENCES

(1) Savenije, T. J.; Ferguson, A. J.; Kopidakis, N.; Rumbles, G. Revealing the Dynamics of Charge Carriers in Polymer:Fullerene Blends Using Photoinduced Time-Resolved Microwave Conductivity. *J. Phys. Chem. C* **2013**, *117*, 24085−24103.

(2) Oga, H.; Saeki, A.; Ogomi, Y.; Hayase, S.; Seki, S. Improved understanding of the electronic and energetic landscapes of perovskite solar cells: high local charge carrier mobility, reduced recombination, and extremely shallow traps. *J. Am. Chem. Soc.* **2014**, *136*, 13818−13825.

(3) Kunst, M.; Werner, A. Comparative study of time-resolved conductivity measurements in hydrogenated amorphous silicon. *J. App. Phys.* **1985**, *58*, 2236−2241.

(4) Martin, S. T.; Herrmann, H.; Hoffmann, M. R. Time-resolved microwave conductivity. Part 2.-Quantum-sized TiO2and the effect of adsorbates and light intensity on charge-carrier dynamics. *J. Chem. Soc. Faraday Trans.* **1994**, *90*, 3323−3330.

(5) Nelson, J. A. *The Physics of Solar Cells*; Imperial College Press, 2003.

(6) Herz, L. M. Charge-carrier mobilities in metal halide perovskites: fundamental mechanisms and limits. *ACS Energy Lett.* **2017**, *2*, 1539−1548.

(7) Herz, L. M. Charge-carrier dynamics in organic-inorganic metal halide perovskites. *Annu. Rev. Phys. Chem.* **2016**, *67*, 65−89.

(8) Binh, N. T.; Minh, L. Q.; Bässler, H. Photoconduction in poly(3-alkylthiophene) II. Charge transport. *Syn. Met.* **1993**, *58*, 39−50.

(9) Hoffmann, S. T.; Jaiser, F.; Hayer, A.; Bässler, H.; Unger, T.; Athanasopoulos, S.; Neher, D.; Köhler, A. How do disorder, reorganization, and localization influence the hole mobility in conjugated copolymers? *J. Am. Chem. Soc.* **2013**, *135*, 1772−1782.

(10) Mozer, A. J.; Dennler, G.; Sariciftci, N. S.; Westerling, M.; Pivrikas, A.; Österbacka, R.; Juška, G. Time-dependent mobility and recombination of the photoinduced charge carriers in conjugated polymer/fullerene bulk heterojunction solar cells. *Phys. Rev. B* **2005**, *72*, 035217.

(11) Tan, M. J.; Goh, W. P.; Li, J.; Pundir, G.; Chellappan, V.; Chen, Z. K. Charge mobility and recombination in a new hole transporting polymer and its photovoltaic blend. *ACS App. Mater. Interfaces* **2010**, *2*, 1414−1420.

(12) Shkunov, M.; Simms, R.; Heeney, M.; Tierney, S.; McCulloch, I. Ambipolar Field-Effect Transistors Based on Solution-Processable Blends of Thieno[2,3-b]thiophene Terthiophene Polymer and Methanofullerenes. *Adv. Mater.* **2005**, *17*, 2608−2612.

(13) Deibel, C.; Baumann, A.; Wagenpfahl, A.; Dyakonov, V. Polaron recombination in pristine and annealed bulk heterojunction solar cells. *Synth. Met.* **2009**, *159*, 2345−2347.

(14) Baumann, A.; Savenije, T. J.; Murthy, D. H. K.; Heeney, M.; Dyakonov, V.; Deibel, C. Influence of Phase Segregation on Recombination Dynamics in Organic Bulk-Heterojunction Solar Cells. *Funct. Mater.* **2011**, *21*, 1687−1692.

(15) Chen, S.; Choudhury, K. R.; Subbiah, J.; Amb, C. M.; Reynolds, J. R.; So, F. Photo-Carrier Recombination in Polymer Solar Cells Based on P3HT and Silole-Based Copolymer. *Adv. Energy Mater.* **2011**, *1*, 963−969.

(16) Blom, P. W.; Mihailetchi, V. D.; Koster, L. J. A.; Markov, D. E. Device Physics of Polymer:Fullerene Bulk Heterojunction Solar Cells. *Adv. Mater.* **2007**, *19*, 1551−1566.

(17) Pivrikas, A.; Sariciftci, N. S.; Juška, G.; Österbacka, R. A review of charge transport and recombination in polymer/fullerene organic solar cells. *Prog. Photovolt.* **2007**, *15*, 677−696.
(18) Saeki, A.; Yasutani, Y.; Oga, H.; Seki, S. Frequency-Modulated Gigahertz Complex Conductivity of TiO2 Nanoparticles: Interplay of Free and Shallowly Trapped Electrons. *J. Phys. Chem. C* **2014**, *118*, 22561−22572.
(19) Fravventura, M. C.; Deligiannis, D.; Schins, J. M.; Siebbeles, L. D.; Savenije, T. J. What Limits Photoconductance in Anatase TiO2 Nanostructures? A Real and Imaginary Microwave Conductance Study. *J. Phys. Chem. C* **2013**, *117*, 8032−8040.
(20) Ferguson, A. J.; Kopidakis, N.; Shaheen, S. E.; Rumbles, G. Dark Carriers, Trapping, and Activation Control of Carrier Recombination in Neat P3HT and P3HT:PCBM Blends. *J. Phys. Chem. C* **2011**, *115*, 23134−23148.
(21) Guse, J. A.; Jones, T. W.; Danos, A.; McCamey, D. R. Recombination dynamics in thin-film photovoltaic materials via time-resolved microwave conductivity. *JoVE* **2017**, *121*, 55232.
(22) Shrestha, P. R.; Abhyankar, N.; Anders, M. A.; Cheung, K. P.; Gougelet, R.; Ryan, J. T.; Szalai, V.; Campbell, J. P. Nonresonant transmission line probe for sensitive interferometric electron spin resonance detection. *Anal. Chem.* **2019**, *91*, 11108−11115.
(23) Wieghold, S.; Bieber, A. S.; VanOrman, Z. A.; Daley, L.; Leger, M.; Correa-Baena, J. P.; Nienhaus, L. Triplet sensitization by lead halide perovskite thin films for efficient solid-state photon upconversion at subsolar fluxes. *Matter* **2019**, *1*, 705−719.
(24) Pace, N. A.; Korovina, N. V.; Clikeman, T. T.; Holliday, S.; Granger, D. B.; Carroll, G. M.; Nanayakkara, S. U.; Anthony, J. E.; McCulloch, I.; Strauss, S. H.; Boltalina, O. V.; Johnson, J. C.; Rumbles, G.; Reid, O. G. Slow charge transfer from pentacene triplet states at the Marcus optimum. *Nat. Chem.* **2020**, *12*, 63−70.
(25) Pace, N. A.; Clikeman, T. T.; Strauss, S. H.; Boltalina, O. V.; Johnson, J. C.; Rumbles, G.; Reid, O. G. Triplet excitons in pentacene are intrinsically difficult to dissociate via charge transfer. *J. Phys. Chem. C* **2020**, *124*, 26153−26164.
(26) Wilson, J. N.; Frost, J. M.; Wallace, S. K.; Walsh, A. Dielectric and ferroic properties of metal halide perovskites. *APL Mater.* **2019**, *7*, 010901−010914.
(27) Hong, M. J.; Zhu, L.; Chen, C.; Tang, L.; Lin, Y. H.; Li, W.; Johnson, R.; Chattopadhyay, S.; Snaith, H. J.; Fang, C.; Labram, J. G. Time-resolved changes in dielectric constant of metal halide perovskites under illumination. *JACS* **2020**, *142*, 19799−19803.
(28) Juarez-Perez, E. J.; Sanchez, R. S.; Badia, L.; Garcia-Belmonte, G.; Kang, Y. S.; Mora-Sero, I.; Bisquert, J. Photoinduced giant dielectric constant in lead halide perovskite solar cells. *J. Phys. Chem. Lett.* **2014**, *5*, 2390−2394.
(29) *Dynamics During Spectroscopic Transitions: Basic Concepts*; Lippert, E., Macomber, J. D., Eds. ; Springer Science & Business Media, 2012.
(30) Poole, C. P. *Electron Spin Resonance: a Comprehensive Treatise on Experimental Techniques*, 2nd ed.; Wiley: NewYork, 1983.
(31) Marshall, A. G. Dispersion vs. absorption (DISPA): A magic circle for spectroscopic line shape analysis. *Chemom. Intell. Lab. Syst.* **1988**, *3*, 261−275.

https://doi.org/10.1021/acs.jpcc.2c08700
J. Phys. Chem. C 2023, 127, 4203−4209